ANL/CHM/PP--90254

Speciation of Uranium in Surface-Modified, Hydrothermally Treated, $(UO_2)^{2+}$-Exchanged Smectite Clays

D. M. Giaquinta, L. Soderholm, S. E. Yuchs and S. R. Wasserman

Chemistry Division, Argonne National Laboratory, Argonne, IL 60439-4831

ABSTRACT

X-ray absorption spectroscopy (XAS) is used to determine the uranium speciation in exchanged and surface-modified clays. The XAS data from uranyl-loaded bentonite clay are compared with those obtained after the particle surfaces have been coated with alkylsilanes. These silane films, which render the surface of the clay hydrophobic, are added in order to minimize the ability of external water to exchange with the water in the clay interlayer, thereby decreasing the release rate of the exchanged-uranium species. Mild hydrothermal conditions are used in an effort to mimic potential geologic conditions that may occur during long-term radioactive waste storage. The XAS spectra indicate that the uranyl monomer species remain unchanged in most samples, except in those samples that were both coated with an alkylsilane and hydrothermally treated. When the clay was coated with an organic film, formed by the acidic deposition of octadecyltrimethoxysilane, hydrothermal treatment results in the formation of aggregated uranium species in which the

uranium is reduced from U^{VI} to U^{IV}. The implications of this reduction to efforts in environmental remediation are discussed.

KEYWORDS: uranium, uranyl, EXAFS, clay, remediation, environment

INTRODUCTION

A successful solution to the problem of disposal and permanent storage of water soluble radioactive species must address two issues: exclusion of the radionuclides from the environment and the prevention of leaching from the storage media into the environment. Recently, immobilization of radionuclides in glasses [1-5], ceramics [6,7] and clay minerals [8-13] has been studied. Clay minerals are of interest in part because they readily exchange cations into their interlayers [14] and in part because smectite clays occur as decomposition products in the leach layers of borosilicate glasses [15]. In addition to the study of clays as potential waste forms, they are also important because they have a ubiquitous presence in the environment. Information about the interactions of radionuclides with clays and how such interactions affect their speciations is crucial for successful modeling of actinide-migration [16].

Smectite clay minerals are 2:1 layer structures. They are composed of crystalline sheets of octahedrally coordinated cations, usually Al^{3+}, that share oxygen atoms with two tetrahedrally coordinated sheets of Si^{4+}. The sheets are separated by an interlayer space or gallery which is populated by cations and water.(Figure 1) Substitutions of octahedrally coordinated Mg^{2+} for Al^{3+} create a localized negative charge in the lattice that is balanced by the cations in the interlayer. These interlayer cations are hydrated and, under appropriate conditions, can be easily exchanged with cations external to the clay. Clays are hydrophilic and their degree of hydration depends on the ambient conditions to which the clay is exposed. The minerals swell upon exposure to excess water by reversibly taking up

water into the interlayer [14,17]. Heating in a dry atmosphere will remove this excess water [18]. The degree of hydration within the interlayer can be estimated by using X-ray diffraction to monitor the distance between the clay layers [19].

The ion-exchange capacity, stability under hydrothermal conditions, and swelling properties of smectite clays have been well studied [10,11,13,20-23]. The smectites have sufficient ion-exchange capacity and hydrothermal stability properties to be viable as long term storage media for hazardous waste under relevant natural conditions: low concentrations of uranium and moderate temperatures and pressures [11,12,22]. Because clays are hydrophilic, however, potential leaching of uranium from a clay into the groundwater is a major concern. In order to reduce the severity of such leaching of the stored ion from the clay, the affinity of external water for the mineral surface and the interlayer must be minimized.

One approach to reducing exchange of the interlayer water and ions, with the groundwater is through a surface modification of the clay. This modification can be accomplished by coating the naturally hydrophilic clay with a hydrophobic layer, such as that produced by a long-chain organosilane. The silanes bond covalently to the surface of the clay mineral, resulting in the formation of a permanently anchored thin film. The resulting hydrophobic coating has been demonstrated to inhibit the exchange between external and interlayer water and associated ions [24], thereby reducing the leaching rate of exchanged ions from the interlayer back into the groundwater.

In this paper we describe the effect of surface modification on the speciation of uranyl cations within the interlayer of a smectite clay, bentonite. Two different silanes are examined, a trimethoxy- and a trichloro-silane, both with linear alkyl chains which contain 18 carbon atoms. Selected samples have been hydrothermally treated in order to simulate potential repository conditions [25] and to determine how these conditions may effect uranyl speciation in exchanged clays. This study relies primarily on X-ray absorption spectroscopy (XAS) to elucidate the local structure of the uranium species in the interlayer space, and to determine the chemical and physical changes that are experienced by these moieties during hydrothermal treatment.

EXPERIMENTAL SECTION

Loading of uranyl into clay interlayer

The Ca^{2+} form of bentonite, bentolite L (Southern Clay Products), was used as received. 50 mM uranyl nitrate solutions were prepared from uranyl nitrate, $(UO_2)(NO_3)_2 \cdot 6H_2O$ (Mallinckrodt). The clay (2 g) was added to a stirred solution of uranyl nitrate (200 ml). The uranyl nitrate-clay slurry was stirred overnight at room temperature. The slurry was allowed to settle, after which the solid was collected by centrifugation. The clay was washed three times by stirring in deionized water (50 mL) for 5 to 10 minutes to remove any excess uranium. The clays were then dried in air at room temperature in an evaporating dish.

Addition of alkyl silanes to clay surface

The uranyl ion-exchanged bentolite L samples were coated with octadecyltrimethoxysilane, $CH_3(CH_2)_{17}Si(OCH_3)_3$ (Aldrich, denoted as $C_{18}Si(OMe)_3$) and octadecyltrichlorosilane $CH_3(CH_2)_{17}SiCl_3$ (Aldrich, denoted as $C_{18}SiCl_3$). The silanes were vacuum distilled and stored under dry nitrogen prior to use. The clay (1 g) and silane (1 mL) were added to anhydrous hexane (40 ml). The mixture was stirred for 24 hours at room temperature in a dry nitrogen atmosphere. 3-indolepropionic acid (0.01g) was added as a catalyst for the reaction of the trimethoxy silane with the clay surface. The samples were collected by centrifugation and washed three times with anhydrous hexane (25 ml) to remove any unreacted silane. After the final wash, the coated clay was dried at room temperature. The colors of the products were off-white and light purple for the $C_{18}SiCl_3$ and $C_{18}Si(OMe)_3$ samples respectively. The process for the formation of the surface coatings is based on previous work on self-assembled monolayers [26,27].

Hydrothermal treatment

All samples, including the native clay, were treated hydrothermally. A stainless steel Parr high pressure bomb (4746) was loaded with a Teflon® insert that contained clay (250 mg) and deionized water (10 mL). The bomb was placed into a Lindberg crucible furnace and heated at 1° per minute to 200°C. The temperature was maintained at 200°C for 20 hours. These conditions are calculated to produce a pressure in the reaction vessel of 225 psi. After the furnace was cooled radiatively to room temperature, the clay was removed from the bomb and the remaining water allowed to evaporate at room temperature.

Powder X-ray diffraction

Powder X-ray diffraction experiments (PXRD) of pelletized clay samples were acquired on a Scintag PAD V diffractometer using CuKα radiation, λ = 1.54184Å, operating at 1.2kW. Spectra were obtained in the range of 2Θ=2 to 80 ° at a scan rate of 0.25° per minute. Peak positions, relative intensities, and peak shape information were determined using the Scintag peak fitting software. All peak positions were calibrated using the mica NBS-675 high d-spacing X-ray standard. The c-axis lattice spacing, which corresponds to the distance between successive sheets of the clay, was determined using both the (001) and (003) reflections.

X-ray absorption spectroscopy -Background

Each element has one or more characteristic X-ray absorption edges [28]. Because the edge energies are unique to an element, and because the characteristic energies are in the keV range, it is often possible to target elements or their ions *in situ* , in the presence of other species. This single-ion probe can provide information about an ion's valence and coordination environment in a solid, liquid or gas [29]. A spectrum, determined as a function of energy about the edge, is artificially divided into two regions to represent the electronic and scattering processes that occur as X-rays are absorbed. The X-ray absorption near edge spectra (XANES) analyze the intensity of absorption as a function of the energy of the incoming photon. During the absorption process, an inner shell electron is excited into valence orbitals. Therefore, these spectra provide information on the electronic structure of the absorbing atom. In general, the energy at which absorption occurs is modified slightly by the valence and local coordination

environment of the absorbing species. By comparison with model compounds, XANES can be used to determine the valence of a given atom. At energies greater than those involved in the single-ion electronic processes, a free photoelectron is generated, which in turn is scattered by neighboring atoms. This scattering leads to small oscillations in the intensity of X-ray absorption, the Extended X-ray Absorption Fine Structure (EXAFS). The Fourier transform of an EXAFS spectrum represents the local distribution of atoms about the absorbing atom. Analysis of the EXAFS can give estimates of the types of species that surround the ion of interest, the distance of each coordination shell from the central atom, **r**, the number of backscatterers present in each coordination shell, **N**, and the relative degree of disorder for each coordinating species, σ. The relationship between these parameters and the observed EXAFS structure as a function of the wave-vector, k, is given by

$$\chi(k) = \sum_j \frac{N_j F_j(k) e^{-2\sigma_j k^2} \sin(2kr_j + \phi_{ij}(k))}{kr_j^2}$$

The total EXAFS measured is a sum of the backscattering from each coordination shell. The backscattering amplitudes, $F_j(k)$, depend only on the backscattering ions whereas the phase shifts, $\phi_{ij}(k)$, are also dependent on the type of ion that absorbs the incoming X-ray photon. These functions are determined either by analysis of the EXAFS from reference compounds or are calculated theoretically using programs such as Feff [30].

X-ray absorption spectroscopy -Experiments

Uranium-loaded clay samples were finely ground, placed in aluminum sample holders (0.25 mm in thickness), and sealed with Kapton® tape. Uranium L_{III}-edge (17166eV) [31] X-ray absorption spectra were obtained at the National Synchrotron Light Source (NSLS) on beamline X23A2. The beamline was equipped with a double-crystal Si <311> monochromator. The entrance slit to the monochromator was set to a 1 mm vertical opening. Data were collected in fluorescence mode using a flow-type fluorescent ion chamber detector (The EXAFS Co.) [32] that was purged with Kr gas. A 3 absorption length strontium filter was placed between the sample and the ion chamber to minimize artifacts caused by scattering of the incident X-ray beam. Calibration of the U L_{III}-edge was maintained by simultaneously measuring the transmission spectrum of sodium uranyl acetate. The energy of the first inflection on the absorption edge of the calibration spectrum was assigned a value of 17166eV. Each reported spectrum is an average of at least two scans.

The EXAFS data were extracted from the absorption spectra using standard procedures [29,33]. The background before the absorption edge was fit to a linear function. The background above the absorption edge was represented by three cubic spline segments. The segments spanned equal ranges in energy space (eV). All transforms and fitting of the EXAFS spectra were performed on the k^3-weighted data. The limits in k-space for the Fourier transform of the EXAFS to the radial structure function were 2.5-11 $Å^{-1}$. The limits in R-space for backtransforms to the k (EXAFS) space are listed in Table II. Data manipulation and fitting were performed using XAMath [34], a package for XAS analysis based on Mathematica®.

Theoretical scattering factors and phase shifts for fitting of EXAFS that arises from the uranium-oxygen and uranium-uranium atom pairs were calculated using Feff 3.25 [30]. Sodium uranyl acetate was used as a standard to determine the amplitude reduction factor, S_0^2, which corrects for errors in the absolute magnitude in the Feff scattering factors. S_0^2 as determined from sodium uranyl acetate was applied to all samples. The energy shift term, ΔE_0, adjusts for differences in the Fermi level in the material and that used in the Feff calculation. For each sample, the energy shift term was determined from the first coordination shell, and then fixed for all additional shells, as has been done previously [35]. Fourier transforms of k^2-weighted EXAFS, $k^2\chi(k)$, and k^3-weighted EXAFS, $k^3\chi(k)$, were compared to determine if high Z elements (uranium in these systems) were involved in backscattering. In only one instance could the feature in the radial structure function be attributed to uranium.

RESULTS

Powder X-ray Diffraction

The powder X-ray diffraction patterns from all of the samples are qualitatively similar. Neither hydrothermal treatment nor surface modification induces major structural changes in the clay. Hydrothermal treatment of the native clay does cause a slight expansion in the c-axis. This observation, which indicates an increased average distance between successive sheets of the clay, may reflect a slight increase in the number of water molecules located within the interlayer. A slight contraction of the c-axis (0.3Å) when $(UO_2)^{2+}$ replaces Ca^{2+} is observed. This result agrees with previous reports [10]. Hydrothermal treatment of the uranyl clays

results in a further decrease in the spacing between the clay sheets. This contraction is greater when the alkylsilane is present on the surface of the uranyl-clay. After hydrothermal treatment, the diffraction peaks broaden considerably and decrease somewhat in intensity. These changes may result from some degradation in the regularity of sheet-to-sheet spacing in the clay, although a slight loss in diffraction intensity may expected from the coated samples because of absorption by the organic coating.

Three different types of EXAFS patterns have been observed in this study depending on the history of the sample. The origins of these three different types of spectra are depicted in terms of sample histories in Figure 2. The $(UO_2)^{2+}$-loaded clays, before and after hydrothermal treatment, and the silane coated clays prior to hydrothermal treatment all have similar EXAFS spectra. These spectra, represented in Figure 3 by the data from the uncoated uranyl-exchanged clay, are adequately represented by three coordination shells. The first two shells are typical of uranyl species: two axial oxygen atoms are present at 1.77Å with 5 equatorial outer shell oxygen atoms at approximately 2.43Å. An additional shell is present at 3.45Å. Whereas we cannot distinguish between Al, Si or oxygen as the backscattering ion in this case, the structure of the interlayer environment suggests that this feature is due to oxygen. The Debye-Waller factors are consistent with those reported in the literature for other uranyl systems [13,23,36-38]. The structural parameters determined from fitting of the EXAFS spectra are listed in Table II.

Both a silane coating and hydrothermal treatment are necessary to produce changes in the local uranium environment from that of the initial, ion exchanged clay. The EXAFS spectra from the $C_{18}SiCl_3$-coated,

hydrothermally treated sample, and the $C_{18}Si(OMe)_3$-coated, hydrothermally treated sample, both show evidence of longer range order about the uranium (Figures 4 and 5). The changes induced by hydrothermal treatment of the $C_{18}SiCl_3$-coated, hydrothermally treated sample are relatively small. Uranyl-type coordination at both the axial and equatorial positions remain, although the observed EXAFS is somewhat lower in intensity. The best fit suggests that the Debye-Waller factors are somewhat larger than those before hydrothermal treatment, however other factors may be involved. There are two additional coordination shells, at 3.59Å and 3.90Å assuming oxygen backscattering.

Hydrothermal treatment of the octadecyltrimethoxysilane-coated clay results in dramatic changes in the uranium environment. The typical axial and equatorial oxygen contacts of the uranyl cation disappear. They are replaced by a single oxygen shell at 2.33Å, with a coordination number of 6. Two additional peaks also appear in the radial distribution. We attribute the first of these peaks to an oxygen shell at 3.36 Å. The backtransform of the second new feature is skewed to higher k, as indicated by the new rapid oscillations in the EXAFS spectra in the region from 7 to 11 $Å^{-1}$. This observation indicates that this peak arises from a nearby high-Z element, which in this system must be uranium. This sample is the only one in which uranium backscattering is clearly evident. It should be noted that although the U-O contact in the $C_{18}SiCl_3$-coated, hydrothermally treated clay is at a similar distance to that assigned to a U-U, details of the data analysis permit the distinction between U-O and U-U.

The XANES spectrum provides further evidence for the type of uranium species that are present in the various uranium-clays. There is an

approximately 3 eV difference in the L_{III} edge energy between tetravalent and hexavalent uranium samples. This value is determined following standard practice [29,33]. The edge shifts of the clays that contain uranyl species are all similar to the spectrum obtained from sodium uranyl acetate. These clays are exemplified in Figure 6b by the spectrum from the untreated uranyl-clay. The maximum in the derivative spectrum occurs at 17,166.5(5) eV. Figure 6 also includes the XANES spectra from the hydrothermally treated $C_{18}SiCl_3$-coated and $C_{18}Si(OMe)_3$-coated samples. The edge of the former is shifted to slightly lower energy, whereas the latter is shifted even lower, to 17,162.4(5) eV, 3.1 eV lower than the hexavalent standard. This shift, together with the coordination environment about the uranium as determined from EXAFS, provide convincing evidence that the $(U^{VI}O_2)^{2+}$ in the methoxy-coated samples, which have undergone hydrothermal treatment, has been reduced to U^{IV}.

DISCUSSION

Two prevalent binding positions have been reported in the literature for smectite clays: external amphoteric sites and internal exchange sites [13]. Previous researchers have reported that the predominant sorption sites in these clays are the interlayer exchange positions [8,12]. However, high coverage of the external sites and high exchange into the interlayer space has been reported when using solution concentrations and pHs similar to those used here [12,13]. Therefore, care was taken to ensure that only internal uranium exchange sites are analyzed in these experiments. Thorough washing was done to remove most, if not all, of the surface-bound and neutral uranium species. Our EXAFS data are successfully analyzed by assuming the presence of only a single type of uranium site

within the interlayer space in all samples. Hydrolysis products such as the dimer $[(UO_2)\cdot(OH)_2\cdot(UO_2)]$ [12] are not observed in uncoated and untreated samples, which is consistent with previous reports [22].

In addition to the two axial oxygen atoms, the uranyl ion has been reported to have an additional 4, 5, or 6 ligands in its inner coordination sphere [39]. In aqueous solutions, a hydration number of 5 is reported for the $(UO_2)^{2+}$ ion [40] although a coordination number of 6 is expected for carbonate or other bidentate ligands [23,37]. The coordination geometry observed for the uranyl ion in the clay samples examined here is consistent with that observed in the aqueous phase, and in other studies of uranyl-clay complexes. The third oxygen contact at 3.45Å, observed for the simple uranyl exchanged clays (Figure 3), is believed to result from the lattice oxygens on the inner clay surface. In combination, the lattice spacing of the clay, the dimensions of the hydrated uranyl species and the third uranium-oxygen contact, suggest that the uranyl unit is "keyed" into the hexagonal hole in the clay-silicate layer, in a manner analogous to that seen for ReO_2^+-exchanged hectorite [41]. In this model, the uranium sits at the center of the hexagonal hole with the axial oxygen atoms oriented along the c-axis perpendicular to the silicon-oxygen planes. The alternative orientation, with the uranyl axial oxygen atoms parallel to the clay plane, is not likely because our powder diffraction patterns indicate that the lattice spacing along the c-axis is on the order of 15 Å. The sheet thickness is 9.6Å [14,17] therefore the height of the interlayer is approximately 5Å. The diameter of the equatorial hydration plane in uranyl is approximately 5Å oxygen to oxygen. Thus, this parallel configuration would require that the uranyl ion be directly bound to the oxygens of the aluminosilicate

sheets in order to be consistent with the diffraction results. We do not believe that such a complexation is reasonable in these systems.

The $C_{18}SiCl_3$-coated, hydrothermally treated system also displays uranyl coordination within the primary coordination shells. The uranyl axial- and equatorial-oxygen distances and coordination numbers are similar to those found in the uncoated samples. However, there are differences in the XANES and EXAFS spectra from this system that may result from the separate or combined effects of aggregation and the presence of chlorine within the interlayer. The oxygen atoms from the lattice appear at a longer distance and have a higher coordination number. An additional contact is also present at 3.90Å. Such long contacts near 4Å may be indicative of uranyl aggregation. Possible aggregate species which are known to form under similar conditions include the uranyl dimer, $(UO_2)_2(OH)_2^{2+}$, and the 3,5 trimer, $(UO_2)_3(OH)_5^{+}$. Comparisons of the radial distribution functions of k^2- and k^3-weighted EXAFS do not show evidence of U-U backscattering, a fact which is more consistent with the 3,5 hydrolysis product. The reported structure of the 3,5 trimer [42] is similar to that of the tri-uranyl carbonate anion, $[(UO_2)_3(CO_3)_6]^{6-}$ [37]. Our EXAFS spectrum of the $C_{18}SiCl_3$-coated, hydrothermally treated system shows qualitative similarities to that of the carbonate compound.

The observed XANES and EXAFS spectra can also be consistent with the presence of chloride ion within the interlayer. The L_{III} absorption-edge XANES from the $C_{18}SiCl_3$-coated sample Figure 6c, shifts approximately 2 eV to lower energy relative to uranyl in the uncoated clay. Although this shift in edge energy could be indicative of a partial reduction of the uranium, the presence of a halogen can slightly shift the edge energy even

without a formal change in valence [43]. Indeed, Feff calculations show that the reduced EXAFS intensity observed from this sample is consistent with the phase cancellation expected with the presence of chlorine. Finally, chlorine has been detected in $C_{18}SiCl_3$-coated clays when the interlayer contains copper(II), nickel(II) and lead(II) [18].

The $C_{18}Si(OMe)_3$-coated, hydrothermally treated sample presents X-ray absorption spectra that are unique among all the samples examined in this study. The near-edge, XANES, spectrum is consistent with tetravalent uranium. The edge energy and shape are indistinguishable from the XANES data from $U^{IV}O_2$. Furthermore, the edge spectra for both this clay and pure UO_2 do not have the shoulder at ≈17185 eV that is found with the uranyl moiety [43]. The EXAFS spectra of uranium in the hydrothermally-treated methoxy-coated clay sample is similar, but not identical, to that obtained from UO_2 [44]. The two short axial oxygen atoms characteristic of $(UO_2)^{2+}$ are clearly absent. The spectrum for uranium in the UO_2, which has the fluorite structure, is consistent with uranium coordinated to 8 oxygen atoms at a distance of 2.33 Å and 12 uranium atoms at 3.87Å [45]. Our EXAFS data (Figure 5) do have a peak at 2.33Å, although the coordination number, 6, is lower than that expected for UO_2. The sample also has a uranium-uranium contact, whose distance, 3.92Å, is similar to that for the corresponding atoms in UO_2. However, as for the first coordination shell, the coordination number, 6, is less than that for the pure oxide. The contact present at 3.36Å is believed to originate from the clay lattice, as described above. Both the XANES and the EXAFS data obtained from the $C_{18}Si(OMe)_3$-coated, hydrothermally treated clay sample are very similar to the spectra from UO_2. These data are consistent

with the formation of UO_2 within the clay interlayer. The reduced coordination numbers, particularly in the second shell, suggests that the uranium has coalesced into small UO_2-like aggregates that have fewer nearest neighbors than are found in extended UO_2. Constraints imposed by the clay interlayer upon aggregation in three dimensions would account for the reduced number of long range contacts.

In these experiments we have found that the presence of an organic, together with elevated temperatures, caused a reduction of uranium from hexavalent (uranyl) to tetravalent. An important question is how strongly reducing an environment exists within such coated clays. It has been previously found that the standard redox potentials determined from solution measurements are comparable, in a relative sense, to those for non aqueous systems, although the absolute potentials may differ between systems. For example, an electromotive force series determined for a variety of ions in glass forming melts is similar to a similar series determined from aqueous solution, differing slightly in detail because of solvent interactions [46]. This concept has been applied in the solid state where E^o values, obtained from solution for a variety of lanthanide and actinide ions, have been used in the synthetic design of complex oxides [47,48]. The redox chemistry of uranium has been extensively studied [45], and has been demonstrated to be pH dependent. In acidic solutions, the uranyl ion is reduced to the +4 oxidation state (equation 1):

$$(UO)_2^{2+} \rightarrow U^{4+} \qquad (1)$$

The reduction potential for this reaction is $E^o = 0.27$ V. In basic solution the reduction of uranyl is more difficult ($E^o = -0.3$ V, equation 2) [49].

$$(UO)_2^{2+}(OH)_2 \rightarrow UO_2 \qquad (2)$$

Although the pH within the interlayer is not known, and would be difficult to measure in the coated samples studied here, a clay interlayer is expected to provide an acidic environment [14]. The EXAFS obtained from samples that were only hydrothermally treated show no significant reduction, indicating that the exchange site in the clay is not sufficiently acidic to drive the reduction of uranyl. The addition of the silane to the clay surface is expected to perturb the local environment within the interlayer, at least by preventing the free transport of water into and out of the clay. Whereas this latter fact could conceivably lead to an increase in the effective acidity of the interlayer, we do not believe that these perturbations alone drive the reduction of the uranyl within the clay. The uranyl species remains after the addition of the coating. A full study of the exact effects of temperature has not yet been performed, but preliminary studies show that the reduction does proceed at lower temperatures [50].

A comparison of standard potentials shows that Cu^{2+} has an E^o value essentially indistinguishable from the one electron reduction of uranyl. The reduction potentials of the reactions:

$$Cu^{2+} + e^- \rightarrow Cu^+$$

and

$$(UO_2)^{2+} + e^- \rightarrow (UO_2)^+$$

are $E^o = 0.159$ [49]. The $(UO_2)^+$ cation disproportionates in solution to yield U^{IV} and $(UO_2)^{2+}$ [45]. Support for the uranyl reduction in our coated clay comes from the observation of similar reduction chemistry

with copper(II) ions [18]. Cu^{2+} that has been ion exchanged into bentonite is reduced either upon heating in nitrogen when there is an organic coating present, or when an uncoated Cu(II)-clay is heated under a reducing atmosphere such as hydrogen. Little if any reduction of Cu occurs when an uncoated clay is heated to similar temperatures under N_2 [18].

The apparent reduction of uranium from hexavalent in the uncoated $(UO_2)^{2+}$-exchanged clays to tetravalent in the methoxy silane coated, hydrothermally-treated clays has potential significance for the understanding of the behavior of uranium under environmentally relevant conditions. An efficient mechanism for the transport of actinide ions in the environment involves their dissolution. Whereas the uranyl ion is very soluble in the slightly acidic aqueous solutions representative of many environments, the tetravalent U^{4+} ion is very insoluble. It will usually precipitate out as the oxide, phosphate or silicate [51]. For example, the geology of the vanadium-uranium deposits in southwestern Colorado has previously been attributed to a low oxidation potential (Eh) environment established by organic matter.[52] Soluble organic materials introduced into groundwater by thermal maturation of humic substances, at temperatures above 80°C, have been proposed to have caused the reduction of vanadium and uranium. These reduced ions were then precipitated as oxides, hydroxides or precursor clay minerals.[53] Our results support this proposed mechanism. Thus a mechanism to reduce the uranyl ion under environmentally relevant conditions has significant potential to limit transport of this potentially dangerous material. We conclude that both clay and an organic are necessary to effect this reduction, together with some mild heating. Our results suggest that adding clay and some organic

material to a contamination site may be a viable method for remediation of contaminated sites. Further work is necessary to evaluate the potential use of such a technique.

ACKNOWLEDGMENTS

The authors thank Dr. J. Woicik and Dr. Mark R. Antonio for technical assistance and Dr. James Sullivan for insightful discussions. This research was supported by the U.S. DOE-Basic Energy Sciences, Chemical Sciences, under contract W-31-109-ENG-38 and the Strategic Environmental Research and Development Program, U.S. DOD.

REFERENCES

1. G. Calas, G.E.J. Brown, G.A. Waychunas, and J. Petiau, Phys. Chem. Minerals, **15** (1987) 19-29.

2. J. Petiau, G. Calas, D. Petit-Maire, A. Bianconi, M. Benfatto, and A. Marcelli, J. Physique, **47** (1986) 949-953.

3. D. Petit-Maire, J. Petiau, G. Calas, and N. Jacquet-Francillon, J. Physique, **47** (1986) 849-852.

4. A.J.G. Ellison, J.J. Mazer, and W.L. Ebert, *Effect of Glass Composition on Waste Form Durability: A Critical Review* 1994, Argonne National Laboratory Report: 94/28.

5. J.K. Bates, A.J.G. Ellison, J.W. Energy, and J.C. Hoh, Materials Research Society Meeting-Nov. 27-Dec.1,1995, Boston, MA, in press.

6. L.W. Hobbs, F.W. Clinard, S.J. Zinkle, and R.C. Ewing, J. Nucl. Mater., **216** (1994) 291-321.

7. E.R. Vance, C.J. Ball, R.A. Day, K.L. Smith, M.G. Blackford, B.D. Begg, and P.J. Angel, J. Alloys Cmpds., **213** (1994) 406-409.

8. L.L. Ames, J.E. McGarrah, B.A. Walker, and P.F. Salter, Chem. Geol., **35** (1982) 205-225.

9. L.L. Ames, J.E. McGarrah, and B.A. Walker, Clays Clay Minerals, **31** (1983) 321-334.

10. Z. Borovec, Chem. Geol., **32** (1981) 45-58.

11. S.E. Miller, G.R. Heath, and R.D. Gonzalez, Clays Clay Minerals, **30**(2) (1982) 111-122.

12. A. Tsunashima, G.W. Brindley, and M. Bastovanov, Clays Clay Minerals, **29** (1981) 10-16.

13. C. Chisholm-Brause, S.D. Conradson, C.T. Buscher, P.G. Eller, and D.E. Morris, Geochim. Cosmochim. Acta, **58**(17) (1994) 3625-3631.

14. R.E. Grim, *Clay Mineralogy, 2nd ed.* 1968, New York: McGraw-Hill.

15. J.K. Bates, W.L. Ebert, X. Feng, and W.L. Bourcier, J. Nucl. Mater., **190** (1992) 198-227.

16. *Molecular Environmental Science: Speciation, Reactivity, and Mobility of Environmental Contaminants*. in *Report of DOE Molecular Science Workshop*. 1995. July 5-8, 1995, Airlie Center, VA.

17. S. Karaborni, B. Smit, W. Heidug, J. Urai, and E. vanOort, Science, **271** (1996) 1102-1104.

18. S.R. Wasserman and S.E. Yuchs, Argonne National Laboratory, unpublished results.

19. *Chemistry of Clays and Clay Minerals*. Mineralogical Society Monograph, ed. A.C.D. Newman. Vol. 6. 1987, New York: Wiley-Interscience.

20. R.B. Heimann, Clays Clay Minerals, **41**(6) (1993) 718-725.

21. H. Yamada and H. Nakazawa, Clays Clay Minerals, **41**(6) (1993) 726-730.

22. D.E. Morris, C.J. Chisholm-Brause, M.E. Barr, S.D. Conradson, and P.G. Eller, Geochim. Cosmochim. Acta, **58**(17) (1994) 3613-3623.

23. A.J. Dent, J.D. Ramsay, and S.W. Swanton, J. Colloid Interf. Sci., **150**(1) (1992) 45-60.

24. S.R. Wasserman, K.B. Anderson, K. Song, S.E. Yuchs, and C.L. Marshall, *Method for Encapsulating and Isolating Hazardous Cations, Medium for Encapsulating and Isolating Hazardous Cations*U.S. Patent Applied For.

25. L.L. Hench, D.E. Clark, and E.L. Yen-Bower, Nucl. Chem. Waste Manag., **1** (1980) 59-75.

26. S.R. Wasserman, Y.-T. Tao, and G.M. Whitesides, Langmuir, **5** (1989) 1074-1087.

27. S.R. Wasserman, G.M. Whitesides, I.M. Tidswell, B.M. Ocko, P.S. Pershan, and J.D. Axe, J. Am. Chem. Soc., **111** (1989) 5852-5861.

28. W.H. McMaster, N. KerrDelGrande, J.H. Mallett, and J.H. Hubbell, *Compilation of X-ray Cross Sections*1969, National Bureau of Standards.

29. B.K. Teo, *EXAFS: Basic Principles and Data Analysis*. 1986, Berlin: Springer-Verlag. Chapter 6.

30. J.Mustre de Leon, J.J. Rehr, S.I. Zabinsky, and R.C. Albers, Phys. Rev. B, **44** (1991) 4146-4156.

31. J.A. Bearden and A.F. Burr, Rev. Mod. Phys., **39** (1967) 125-142.

32. F.W. Lytle, R.B. Greegor, D.R. Sandstrom, E.C. Marques, J.Wong, C.L. Spiro, G.P. Huffman, and F.E. Huggins, Nucl. Instrum. Methods Phys. Res., **226** (1984) 542-548.

33. D.E. Sayers and B.A. Bunder , in *X-ray Absorption: Principles, Applications, Techniques of EXAFS, SEXAFS and XANES,* D.C. Koningsberger and R. Prins, Editors. 1988, John Wiley and Sons: New York. p. Chapter 6.

34. S.R. Wasserman, XAMath is available on the World Wide Web at http://xafsdb.iit.edu:80/exafs-database/programs/XAMath.

35. P.A. O'Day, J.J. Rehr, S.I. Zabinsky, and G.E.J. Brown, J. Am. Chem. Soc., **116** (1994) 2938-2949.

36. H.A. Thompson, G.E. Brown, and G.A. Parks, Physica B, **209** (1995) 167-168.

37. P.G. Allen, J.J. Bucher, D.L. Clark, N.M. Edelstein, S.A. Ekberg, J.W. Gohdes, E.A. Hudson, N. Kaltsotannis, W.W. Lukens, M.P. Neu, P.D. Palmer, T. Reich, D.K. Shuh, C.D. Tait, and B.D. Zwick, Inorg. Chem., **34** (1995) 4797-4807.

38. E.A. Hudson, P.G. Allen, L.J. Terminello, M.A. Denecke, and T. Reich, Phys.Rev. B, in press.

39. H.T.J. Evans, Science, **141** (1963) 154-158.

40. M. Åberg, F. Diego, J. Glaser, and I. Grenthe, Inorg. Chem., **22** (1983) 3986-3989.

41. M.D. Newsham, E.P. Giannelis, T.J. Pinnavaia, and D.G. Nocera, J. Am. Chem. Soc., **110** (1988) 3885-3891.

42. L.M. Toth and G.M. Begun, J. Phys. Chem., **85** (1981) 547-549.

43. E.A. Hudson, J.J. Rehr, and J.J. Bucher, Phys. Rev. B, **52** (1995) 13815-13826.

44. N.T. Barrett, G.N. Greaves, B.T.M. Willis, G.M. Antonini, and F.R. Thornley, J. Phys., **C21** (1988) L791-L796.

45. F. Weigel, in *The Chemistry of the Actinide Elements,* J.J. Katz, G.T. Seaborg, and L.R. Morss, Editors. 1986, Chapman and Hall: Bristol. p. 169-442.

46. H.D. Scheiber and A.L. Hockman, J.Am.Ceram.Soc., **70** (1987) 591-594.

47. L. Soderholm and C.W. Williams , in *Physical and Material Properties of High Temperature Superconductors,* S.K. Malik and S.S. Shah, Editors. 1994, Nova Science: New York. p. 59-76.

48. L. Soderholm, C. Williams, S. Skanthakumar, M.R. Antonio, and S. Conradson, Zeit. Physik B, in press.

49. A.J. Bard, R. Parsons, and J. Jordan, *Standard Potentials in Aqueous Solution.* 1985, New York: Marcel Dekker. pp: 834.

50. D.M. Giaquinta, L. Soderholm, S.E. Yuchs, and S.R. Wasserman, Argonne National Laboratory, unpublished results.

51. J.D. Lee, *Concise Inorganic Chemistry.* 1991, London: Chapman and Hall. pp. 1032.

52. G.N. Breit, Economic Geology, **90** (1995) 407-419.

53. P.L. Hansley and C.S. Spirakis, Economic Geology, **87** (1992) 352-365.

Table II EXAFS Parameters for $(UO_2)^{2+}$-Loaded Clays Before and After Surface Modification and Hydrothermal Treatment.[a]

	$(UO_2)^{2+}$-Bentonite	ht $(UO_2)^{2+}$-Bentonite $C_{18}SiCl_3$-coated	ht $(UO_2)^{2+}$-Bentonite $C_{18}Si(OMe)_3$-coated
shell 1			
N	2.2	2.0	6.3
r	1.77	1.77	2.33
σ	0.0016	0.0042	0.0255
ΔE_0	6.8	8.8	3.5
shell 2			
N	5.0	5.6	2.5
r	2.43	2.44	3.36
σ	0.0085	0.0191	0.0154
shell 3			
N	2.6	6.7	6.1
r	3.45	3.59	3.92
σ	0.0175	0.0270	0.0085
shell 4			
N		3.3	
r		3.90	
σ		0.0074	
R-space limits	1 - 3.6	1 - 4.2	1 - 4.9

[a] Estimated errors associated with EXAFS parameters are 20% for coordination numbers and 2% for distances.

Figure Captions

Figure 1: Layer structure of bentonite.

Figure 2: Reaction scheme for the sequence of surface modification and hydrothermal treatment.

Figure 3: **a** k^3-weighted EXAFS, $k^3\chi(k)$, of $(UO_2)^{2+}$ - bentonite. The best fits are represented by —◇—. * indicates peaks potentially due to uranium-clay interactions.

b Radial distribution of **a**; $\Delta k = 2 - 11 Å^{-1}$. Positions are not corrected for phase.

Figure 4: **a** k^3-weighted EXAFS, $k^3\chi(k)$, of hydrothermally treated, $(UO_2)^{2+}$-bentonite + $C_{18}SiCl_3$. The best fits are represented by —◇—. * indicates peaks potentially due to uranium-clay interactions.

b Radial distribution of **a**; $\Delta k = 2 - 11 Å^{-1}$. Positions are not corrected for phase.

Figure 5: **a** k^3-weighted EXAFS, $k^3\chi(k)$, of hydrothermally treated, $(UO_2)^{2+}$-bentonite + $C_{18}Si(OMe)_3$. The best fits are represented by —◇—. * indicates peaks potentially due to uranium-clay interactions.

b Radial distribution of **a**; $\Delta k = 2 - 11 Å^{-1}$. Positions are not corrected for phase.

Figure 6: **a** XANES of UO_2 (solid line) and sodium uranyl acetate (dotted line).

b XANES of hydrothermally treated,$(UO_2)^{2+}$-bentonite + $C_{18}Si(OMe)_3$ (solid line) and $(UO_2)^{2+}$-bentonite (dotted line).

c XANES of hydrothermally treated,$(UO_2)^{2+}$-bentonite + $C_{18}Si(OMe)_3$ (solid line) and hydrothermally treated,$(UO_2)^{2+}$-bentonite + $C_{18}SiCl_3$ (dotted line).

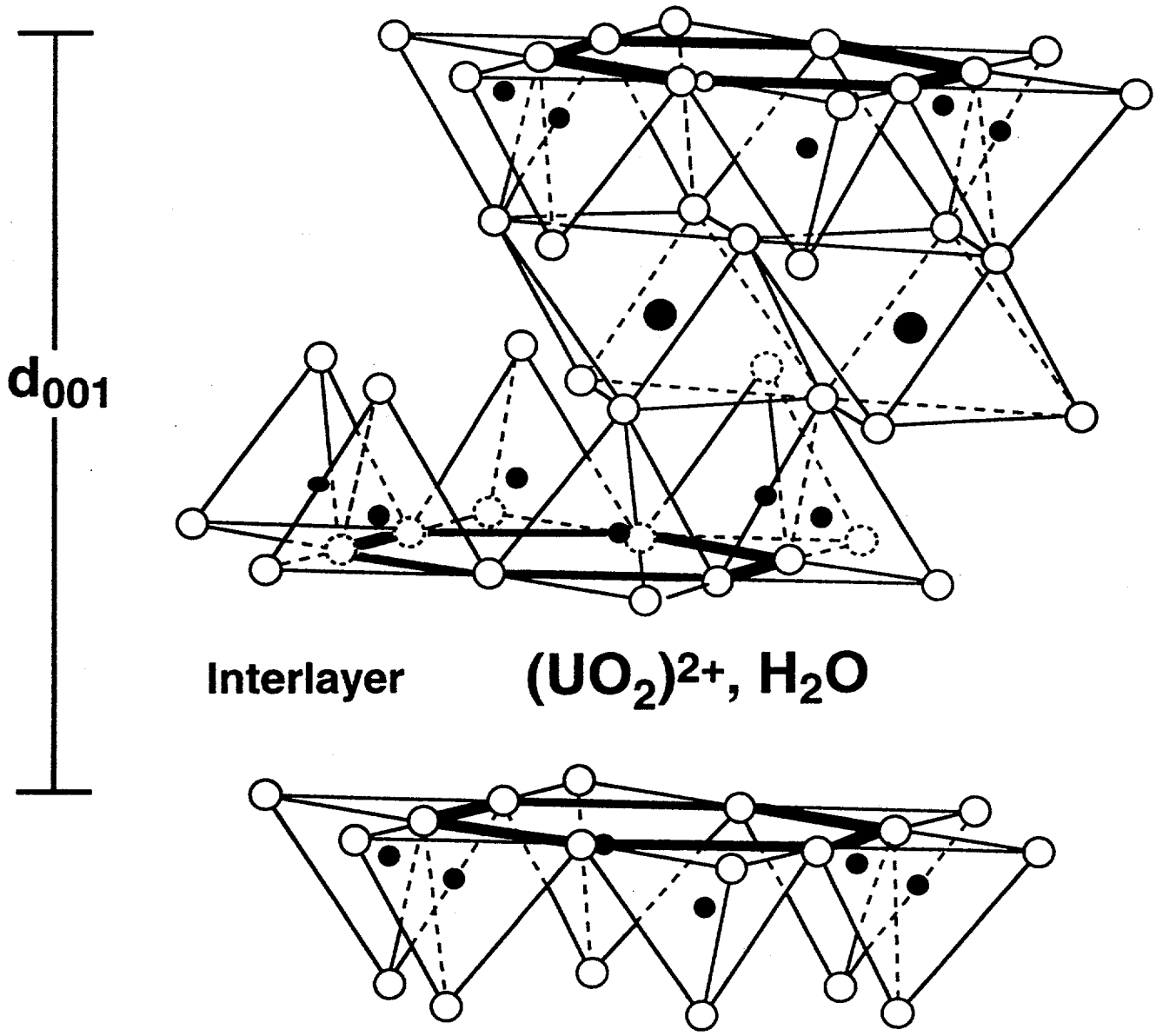

Figure 1

D.M Giaquinta

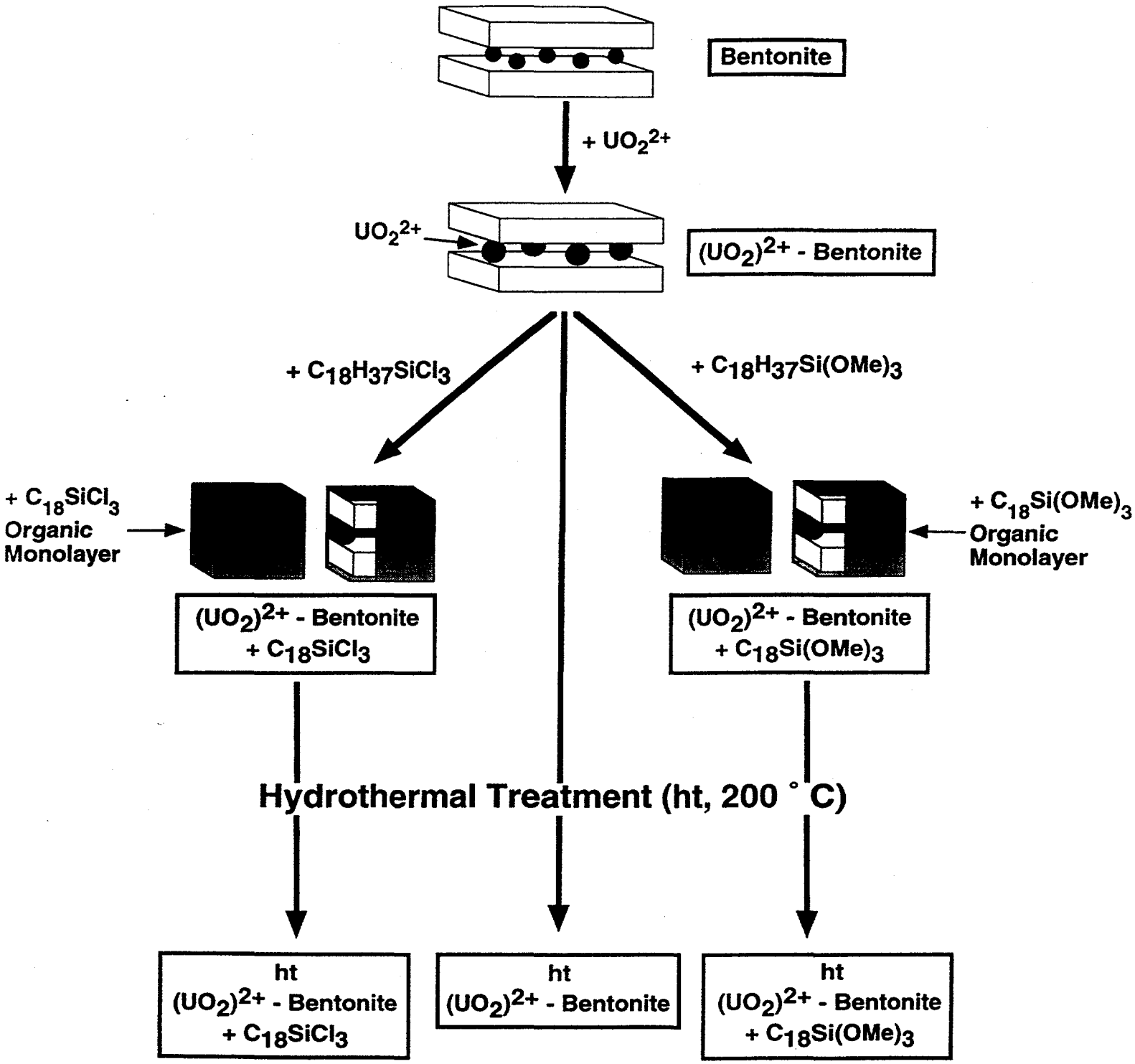

Figure 2

D.M Giaquinta

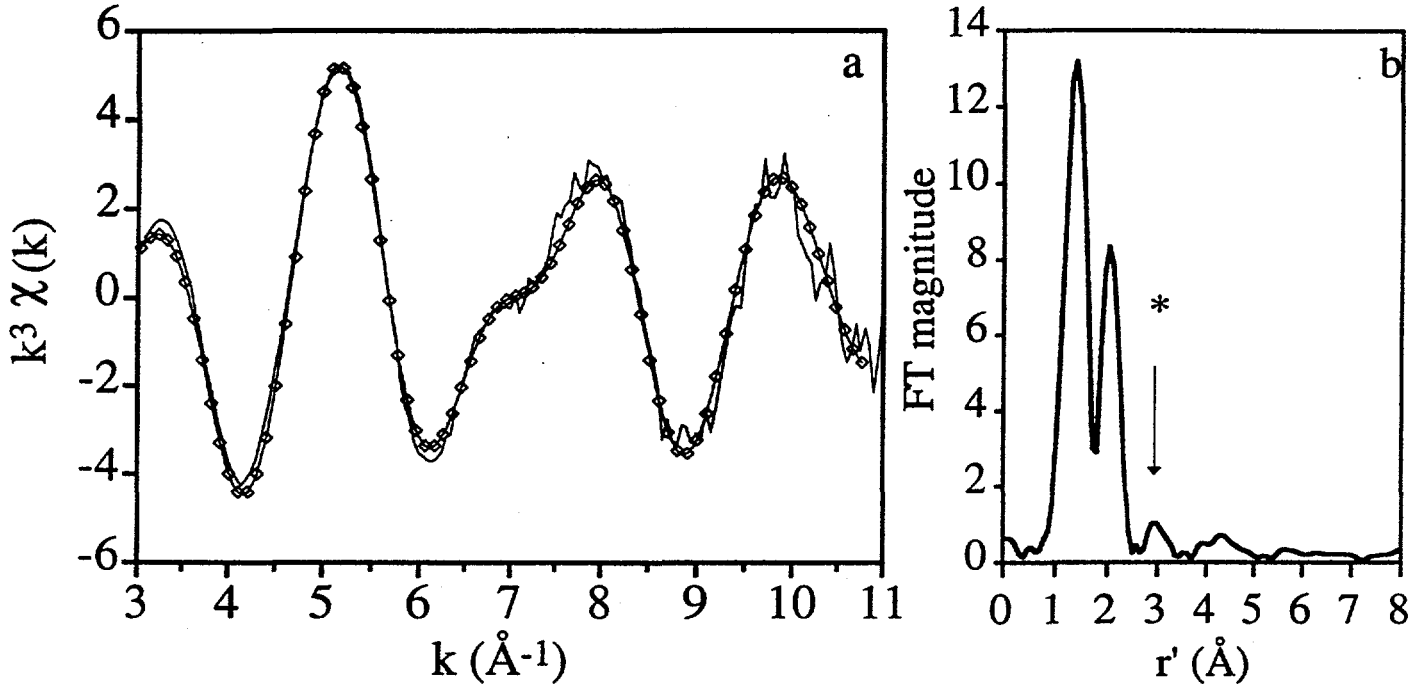

Figure 3

D.M. Giaqu

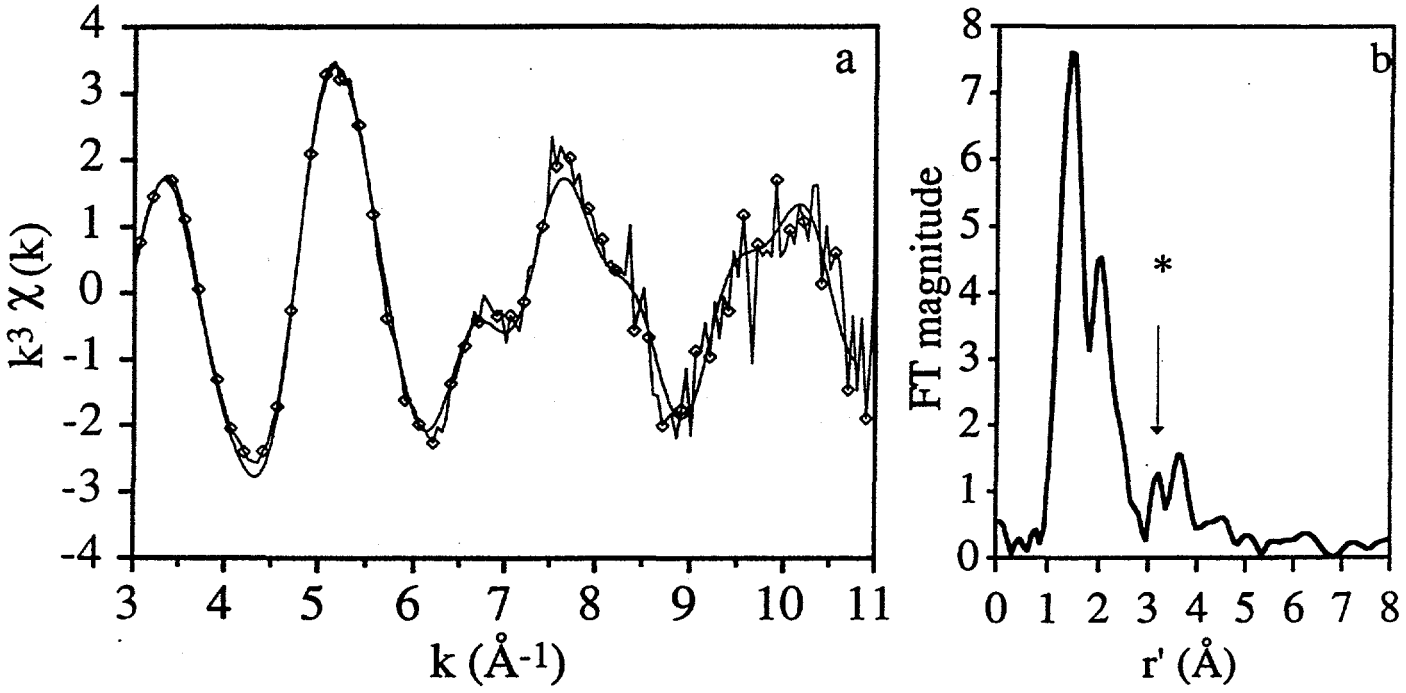

Figure 4

D.T. Gaguila

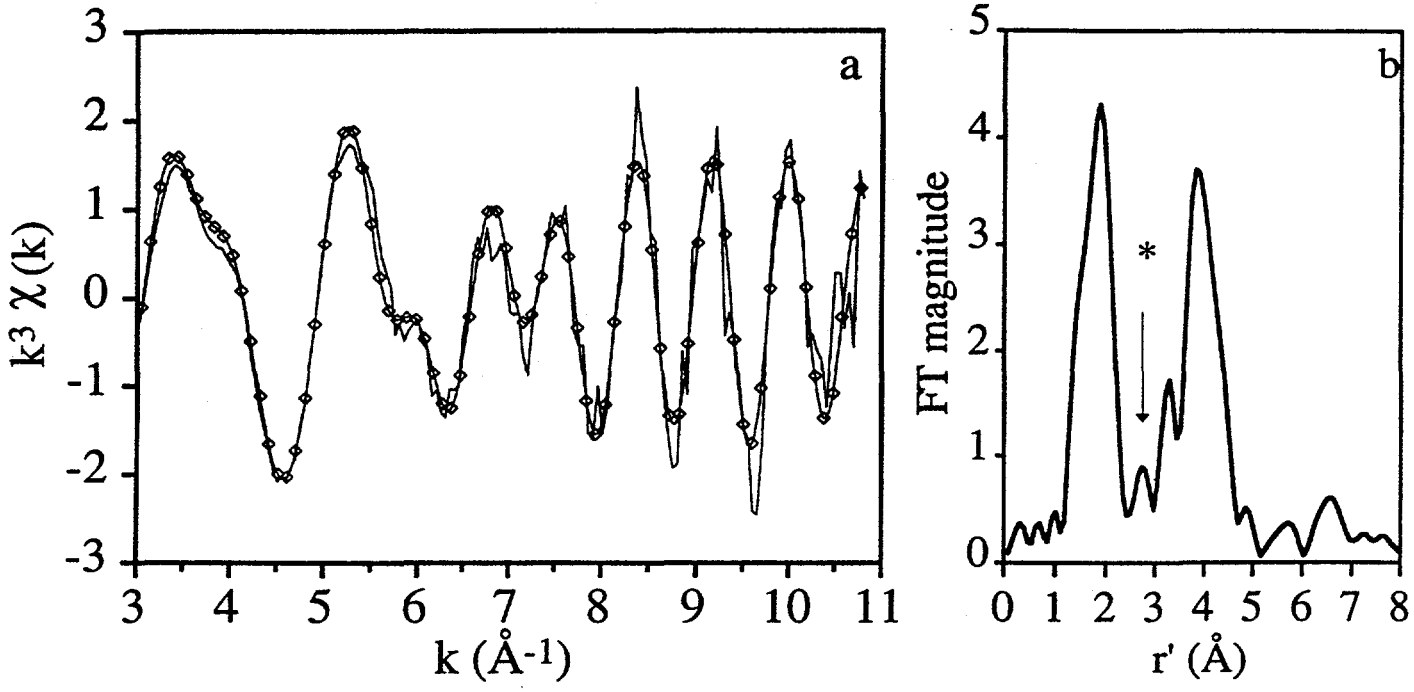

Figure 5 DM Giaquinta

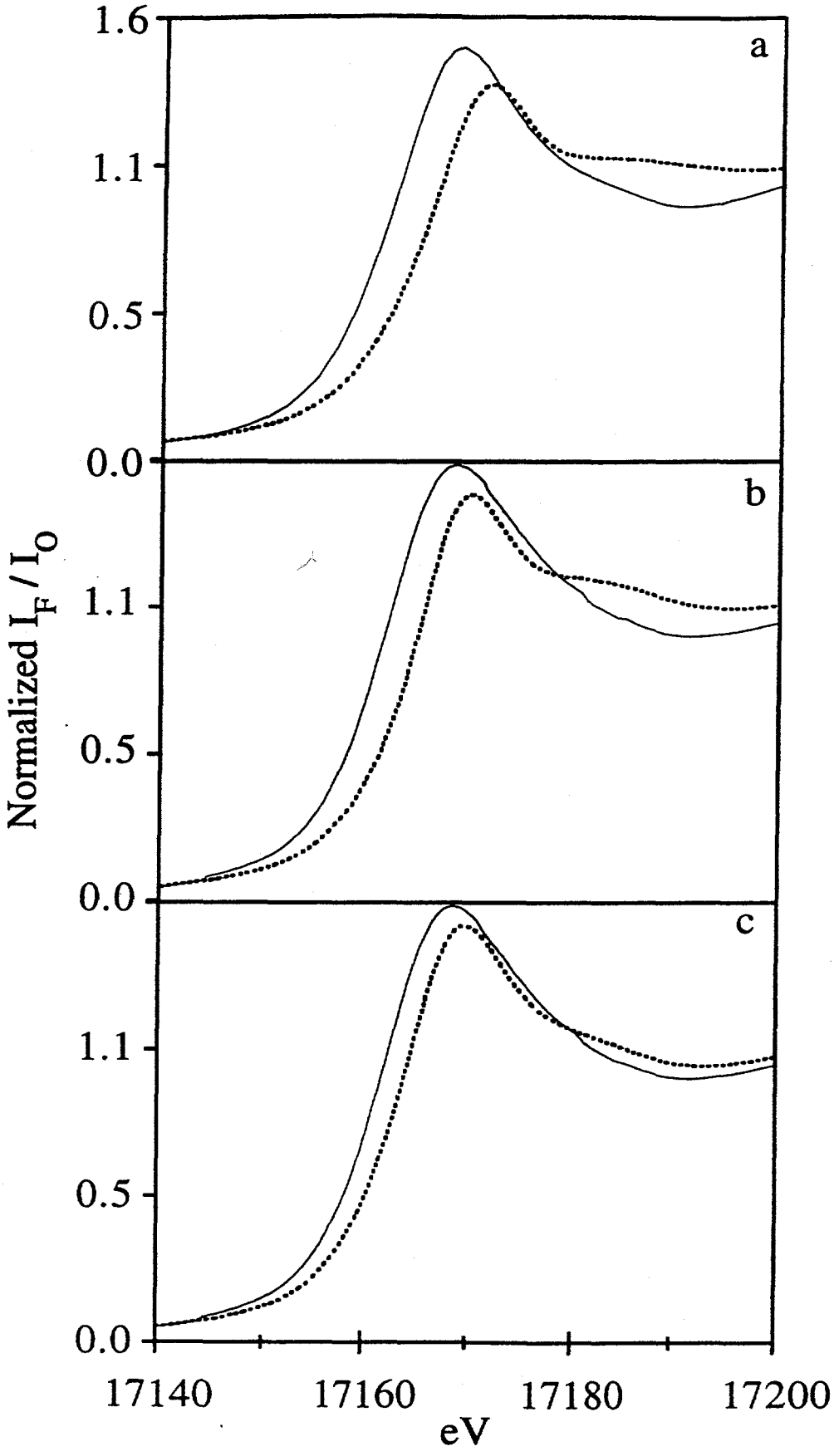

Figure 6 D.M. Giaqu...